JOURNAL OF SYNCHROTRON RADIATION
ISSN 1600-5775

The SASE1 X-ray beam transport system[1]

H. Sinn,[a]* M. Dommach,[a] B. Dickert,[a] M. Di Felice,[a] X. Dong,[b,c] J. Eidam,[a] D. Finze,[a] I. Freijo-Martin,[a] N. Gerasimova,[a] N. Kohlstrunk,[a] D. La Civita,[a] F. Meyn,[a] V. Music,[a] M. Neumann,[a] M. Petrich,[a] B. Rio,[a] L. Samoylova,[a] S. Schmidtchen,[a] M. Störmer,[d] A. Trapp,[a] M. Vannoni,[a] R. Villanueva[a] and F. Yang[a]

[a]European XFEL, Holzkoppel 4, 22869 Schenefeld, Germany, [b]Shanghai Institute of Applied Physics, 239 Zhangheng Road, Shanghai 201204, People's Republic of China, [c]Shanghai Advanced Research Institute, 99 Haike Road, Shanghai 201210, People's Republic of China, and [d]Institute of Materials Research Helmholtz-Zentrum Geesthacht, Zentrum für Material- und Küstenforschung GmbH, Max-Planck-Straße 1, 21502 Geesthacht, Germany. *Correspondence e-mail: harald.sinn@xfel.eu

Received 16 October 2018
Accepted 11 March 2019

Edited by P. Fuoss, SLAC National Accelerator Laboratory, USA

[1] This article will form part of a virtual special issue on X-ray free-electron lasers.

Keywords: XFEL physics; photon beamlines; hard X-rays; beam transport systems; X-ray optical components.

SASE1 is the first beamline of the European XFEL that became operational in 2017. It consists of the SASE1 undulator system, the beam transport system, and the two scientific experiment stations: Single Particles, Clusters, and Biomolecules and Serial Femtosecond Crystallography (SPB/SFX), and Femtosecond X-ray Experiments (FXE). The beam transport system comprises mirrors to offset and guide the beam to the instruments and a set of X-ray optical components to align, manipulate and diagnose the beam. The SASE1 beam transport system is described here in its initial configuration, and results and experiences from the first year of user operation are reported.

1. Introduction

The European XFEL is a free-electron lasing facility based on a superconducting linear accelerator with electron energies up to 17.5 GeV (Altarelli *et al.*, 2006). As the first hard X-ray laser facility based on superconducting technology, it can produce two orders of magnitude more pulses per second than existing hard X-ray lasers. During pulse trains of 600 µs duration, a burst of up to 2700 X-ray pulses with a repetition rate of 4.5 MHz can be produced. Each pulse can have an energy in the millijoule range, leading to a power density during a pulse train of several kW per square millimetre on the optical elements that intercept the beam. In addition to the thermal load, single-shot ablation can occur, where the deposited energy of one X-ray pulse is enough to ablate material from the surface of the beam-intercepting material (Aquila *et al.*, 2015). The combination of single-shot damage and short-term thermal load during the pulse train poses new challenges to the beam transport system. As a consequence, all elements that can intercept the beam are made of thermal conducting low-Z materials, typically boron carbide or diamond.

In May 2017, first lasing was achieved at the European XFEL facility with the SASE1 undulator (Decking *et al.*, 2019). Four months later, the two scientific instruments at the SASE1 beamline, Single Particles, Clusters, and Biomolecules and Serial Femtosecond Crystallography (SPB/SFX; Mancuso *et al.*, 2019), and Femtosecond X-ray Experiments (FXE; Galler *et al.*, 2019), started their user program. Here we describe the general layout of the SASE1 photon-beam transport system (Tschentscher *et al.*, 2017) and its performance as it was used during the first user experiment periods. A detailed description of the beam-transport concepts and its

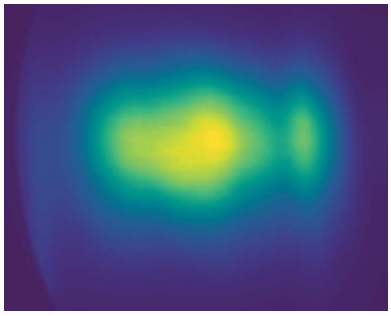

components in the beamline-design phase can be found in the design reports (Sinn *et al.*, 2011, 2012). The diagnostic components that are integrated into the beam transport system are described in more detail by Grünert *et al.* (2019).

2. Beamline design

The SASE1 photon-beam transport system includes all the vacuum systems and the X-ray optical devices that are used to transport the photon beam from the SASE1 undulator (Abeghyan *et al.*, 2019) to the experiments. At SASE1, the photon-beam transport system covers a length of about 1 km and is located in the underground tunnels of the facilities XTD2 and XTD9 and the shaft building XS3. The beamline layout, with its most essential components for beam transport, is shown in Fig. 1. Two important systems that are part of the beam transport system, but are not shown in Fig. 1, are the photon-beam loss monitors (Gerasimova *et al.*, 2014), which can detect and switch off misdirected beams, and the four-bounce silicon (111) monochromator in the FXE branch (Dong *et al.*, 2016). These systems were installed, but were not in operation, during the first user periods and their functions will be described in a later publication.

2.1. Source-point location

The source point at a FEL is typically expected to be located 1–2 Rayleigh lengths before the end of the active undulator section (Samoylova *et al.*, 2014; Manetti *et al.*, 2019). Depending on which undulators are closed for the particular lasing conditions, the source-point position may vary accordingly. In the SASE1 beamline design, we defined a nominal source point in the centre of the third to last undulator module (U33), which is about one Rayleigh length from the end of the undulator at 14 GeV with a fully closed undulator gap. During the first user runs, the last seven undulator modules were, for technical reasons, not used, which means that the physical source point is expected to be 42.7 m upstream of the nominal source point. In the following, we will refer to distances always with respect to the nominal source point.

2.2. Spontaneous radiation apertures

The spontaneous radiation apertures (SRAs) at a distance of 198 m from the nominal source point are the first elements that can intercept the photon beam. The purpose of the SRAs is to cut down the spontaneous radiation background from the X-ray laser beam. This is required to ensure the proper operation of X-ray gas monitor (XGM) systems behind the SRAs and to reduce heat load on the first mirror. The spontaneous radiation background is the non-lasing undulator radiation equivalent to the undulator radiation as used at storage rings. The fundamental of the spontaneous radiation has the same photon energy as the lasing fundamental, but a broader spread in angle and energy and only a few percent of the lasing intensity. However, the higher harmonics of the spontaneous radiation peak at the critical energy of the undulator, which is about 130–200 keV for 14–17.5 GeV electron energy of the accelerator. The total integrated power in the spontaneous radiation at SASE1 can reach up to 1 kW, more than ten times the integrated lasing power. Therefore, the SRA blades consist of 30 mm-thick water-cooled boron carbide blocks that can withstand the tails of the X-ray FEL radiation, followed by 30 mm-thick water-cooled tungsten blocks that can absorb the high-energy spontaneous radiation. The individual blades of the SRA are arranged in a sequence such that they cannot collide when fully closed.

2.3. XGM systems

In the SASE1 beam transport system, two XGM systems are used, one at the beginning of the beam transport behind the SRA and another in the SPB/SFX branch. A detailed description can be found in the works by Grünert *et al.* (2019) and Tiedtke *et al.* (2009); here we just highlight the most important points relevant to the beam transport. The XGMs work on the principle of an ion chamber and are typically

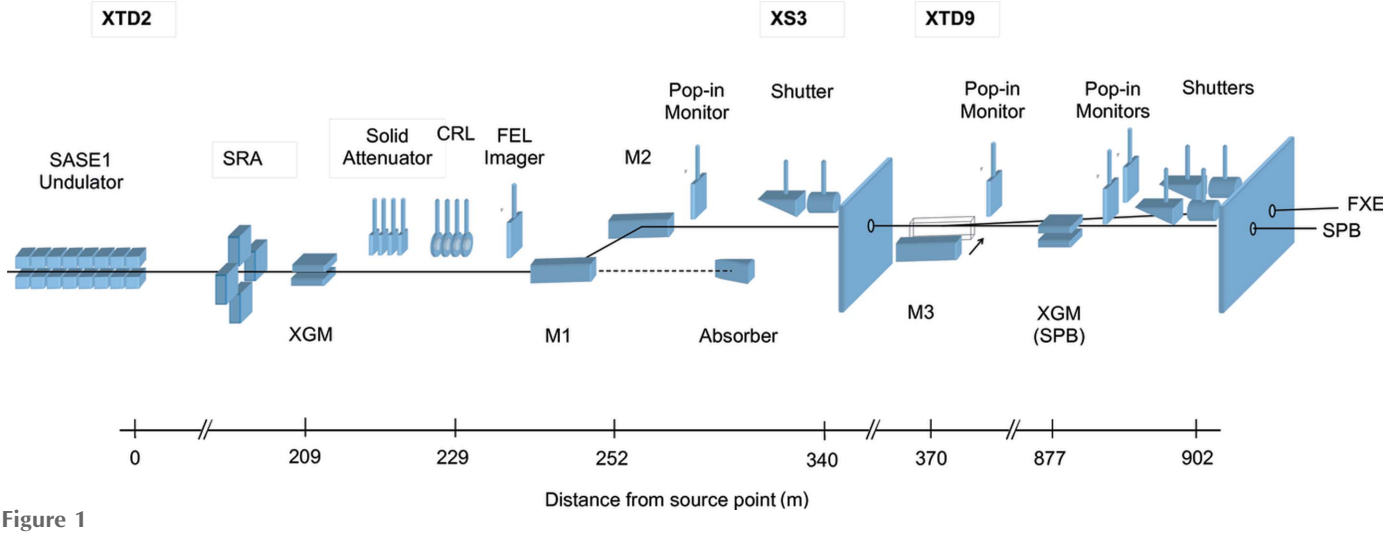

Figure 1
A schematic drawing of the SASE1 beam transport system.

operated in the range of a few 10^{-5} mbar xenon pressure. A calibrated intensity and beam position are derived from the ionic current. To achieve the required absolute precision, these signals are averaged over about 30 s. In addition, a fast signal derived from the photoelectrons is detected, which allows pulse-resolved measurements of intensity and position. These fast signals have to be cross-calibrated to the ion signals whenever the photon energies or the gas pressure of the system are being changed significantly. The XGMs are separated from the beamline vacuum by 6 m-long differential pump sections with a beam aperture of 20 mm.

2.4. Solid attenuator

To attenuate the X-ray FEL intensity, the solid attenuator can be utilized to insert up to nine different actuators equipped with attenuators. The attenuators are polycrystalline chemical vapour deposition diamonds with thicknesses of 75, 150, 300, 600, 1200 and 2400 µm, and aluminium plates of 500 µm, 1 mm and 2 mm thickness. For the 2400 µm-thick diamond, two plates of 1200 µm thickness were stacked together. Polycrystalline materials were used to minimize the risk that strong Bragg reflections could potentially damage sensitive parts of the beam transport. All plates are mounted on heat-conducting copper holders that are passively cooled and monitored with thermocouples. The actuators can be inserted and removed quickly via pneumatic cylinders. Different combinations of attenuators that are required for a desired transmission can be calculated and inserted into the beam by a software tool. At the large distant imagers (*e.g.* pop-in monitors in front of experiments), speckles are visible from the diamond and aluminium plates. Despite these distortions to the beam profile, the average beam position remains the same and can be used for beamline alignment.

2.5. Compound refractive lens system

The compound refractive lens (CRL) (Snigirev *et al.*, 1996) system at 229 m source distance is designed to collimate the X-ray beam (Bressler, 2011). In this way, the beam size can be matched to the acceptance of the CRLs in the FXE hutch (Galler *et al.*, 2019). Also, the CRL system allows the horizontal beam size to be kept within the acceptance of the M3 distribution mirror.

The lenses are made of beryllium and assembled in ten stacks, which can be inserted vertically via step motors into the beam and also have a small horizontal adjustment capability. In front of each lens stack are boron carbide apertures that prevent the beam from hitting anything but the lenses' clear aperture. All lens stacks are water-cooled and monitored for temperature. A local heating of the CRL lenses to above 300°C that can lead to recrystallization effects was excluded by finite element analysis calculations using the operation conditions in 2017/2018.

2.6. Offset mirrors M1 and M2

The offset mirrors M1 and M2 at source distances of 246.5 and 257.86 m, respectively, are part of the radiation-safety concept of the facility. Their purpose is to separate the FEL beam from the high-energy spontaneous background and from bremsstrahlung that could be generated by misdirected electrons in the undulator section hitting an unintended target. As the FEL beam is diffraction limited, its beam size varies considerably over the operation range of the SASE1 beam transport from 3 to 24 keV. The critical angle required to transport 24 keV would lead to a required mirror length of several metres for low photon energies. Therefore, the reflection angle of M1 and M2 is adjustable from 1.1 to 3.6 mrad, leading to a variable beam offset of 25–85 mm. All deflections of SASE1 beam-transport mirrors are in the horizontal plane. During the early user period, the incidence angle used at M1 and M2 was 2.2 mrad at an photon energy of 9.3 keV.

The mirror M2 is bendable by a step-motor-driven U-bender from flat to about 13 km concave bending radius (Freijo Martín *et al.*, 2016; Vannoni, Freijo Martín & Sinn, 2016). The bender has three purposes. Firstly, to achieve a sufficiently flat mirror profile. Currently, the absolute precision in mirror manufacturing allows polishing flat mirrors to a specification of larger than 300–600 km. In the geometry of the SASE1 beam transport, such weak curvatures would still lead to a noticeable undesired focusing effect. By fine-tuning the M2 bender, these potential residual mirror curvatures of M1 and M2 combined can be compensated.

Secondly, with higher beam power, one would expect the mirrors to bend slightly convex, in particular if the mirror cooling is used. All beam-transport mirrors have a water-cooling system with a eutectic indium–gallium interface and were designed to minimize deformations under full thermal load. However, in 2017–2018, these cooling systems were not used for technical reasons. With beam loading of up to 120 pulses per train, no noticeable effect of beam steering or bending caused by heat load were detected.

Finally, bending M2 makes it possible to generate an intermediate horizontal focus behind the M3 distribution mirror. Because M3 has to work at a fixed angle, it is not possible to compensate the variation of beam size at different photon energies by changing the reflection angle. With an intermediate focus of M2 at 430 m, no cutting of the beam occurs over the photon-energy working range, and the horizontal beam size matches the vertical size at the location of the experiments (Sinn *et al.*, 2011).

The M2 bender has, on the backside of the mirror substrate, three capacitive sensors that enable measurement of the bending radius online with some degree of accuracy and enable the observation of possible variations over time (Vannoni, Freijo Martín, Music & Sinn, 2016; Music, 2015).

The SASE1 beam-transport mirrors are located in vacuum chambers ('chambers for horizontal offset mirrors', or CHOMs) as shown in Fig. 2. The design of the CHOMs was developed in collaboration with Helmholtz-Zentrum Berlin (Noll *et al.*, 2009) and originates from the design idea that all motors, gearboxes and spindles potentially outgassing hydrocarbons or generating dust particles are located outside of the vacuum chamber. The actuation scheme is based on parallel

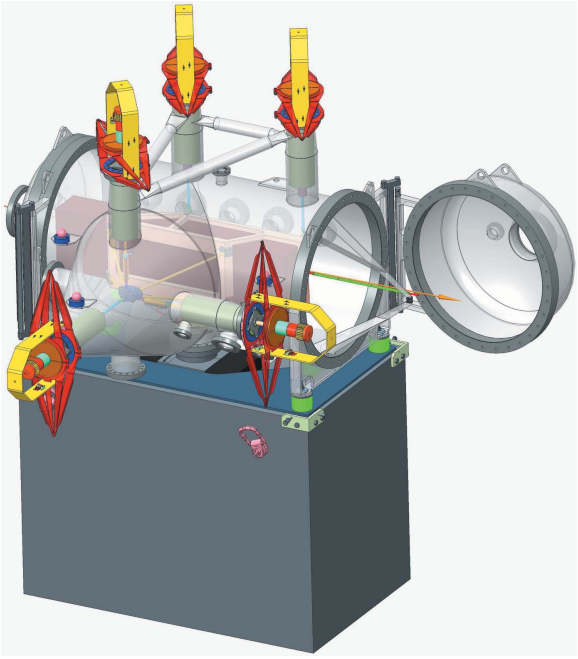

Figure 2
A rendering of the mirror chamber (CHOM) for the M1 and M2 offset mirrors and the M3 distribution mirror. Five degrees of freedom can be manipulated by out-of-vacuum step motors.

kinematic motions (Noll *et al.*, 2016) and minimizes backlashes. The fine-threaded spindles, together with high-ratio planetary gearboxes, lead to a resolution of 67 nm per full step for the less-sensitive degrees of freedom and 19 nm per full step for the pitch motion. When adjusting the pitch angle, steps of 100 nm are routinely performed during the alignment of the instruments, corresponding to about 200 µm beam motion at the location of the instruments with a backlash of less than 1 µm. Smaller adjustments with no noticeable backlash can be made with in-vacuum piezo actuators on the pitch and roll motions of the M2 mirror. Interferometric measurements of the pitch angle yielded a vibration level of 20 nrad r.m.s. (Sinn *et al.*, 2012).

Because of the out-of-vacuum actuation design, the mirror alignment is, in principle, sensitive to short-term temperature drifts and to changes in air pressure. The design of the CHOMs was optimized to minimize these effects on the pitch motion by the geometry of the actuation scheme, an increased wall thickness of the chamber, and by adding stiffeners. However, during the operation phase 2017–2018, drifts on the µrad scale over time windows of about 20 min were observed in certain instances. Investigations to determine if this is caused by deformations of the CHOMs or drifts of the beam itself, and developments to correct this using feedback on the pitch motion piezo, are currently ongoing.

2.7. Distribution mirror M3

The distribution mirror M3 can be inserted by the horizontal translation into the beam path in order to deflect the beam to the FXE instrument. A deflection angle of 1.35 mrad leads to a separation of the two beams of 1.435 m at the end of the photon tunnels, allowing a side-by-side geometry of the two scientific instruments. The 0.9 m-long mirror substrate M3 acts like a 1.2 mm horizontal aperture. Beams with unfocused sizes larger than that can be slightly focused using the collimating CRLs, the M2 bender, or a combination of both in order to fit through the aperture. The M3 mirror is a flat mirror and, like the M2 mirror, is equipped with piezo actuators for pitch and roll motions.

2.8. Shutters

In the shaft building XS3 and at the end of the photon tunnels, shutters are installed to stop the photon beam. The shutter in XS3 enables commissioning activities of the SASE1 undulator or operation of the subsequent SASE3 undulator, while performing work in the XTD9 tunnel. The design of the shutters is shown in Fig. 3. The main shutter component consists of an 8 cm-thick tungsten block that is inserted into the beam path and specified such that it safely stops the high-energy spontaneous radiation. Because the FEL radiation is, in principle, able to ablate the tungsten material, an absorber is inserted before the tungsten shutter every time the shutter closes. The absorber consists of a water-cooled 30 cm-long boron carbide structure that is angled towards the beam with a 10° incidence angle in order to distribute the thermal load. In case the absorber fails, a burn-through monitor is located in between the absorber and the shutter. The burn-through monitor is a volume filled with air and connected to the ambient atmosphere. If the beam were to penetrate through this volume, a vacuum failure would be generated. In addition, a photomultiplier connected via an optical fibre to the air volume of the burn-through monitor would trigger a stop of the injector by detecting the fluorescence induced by the

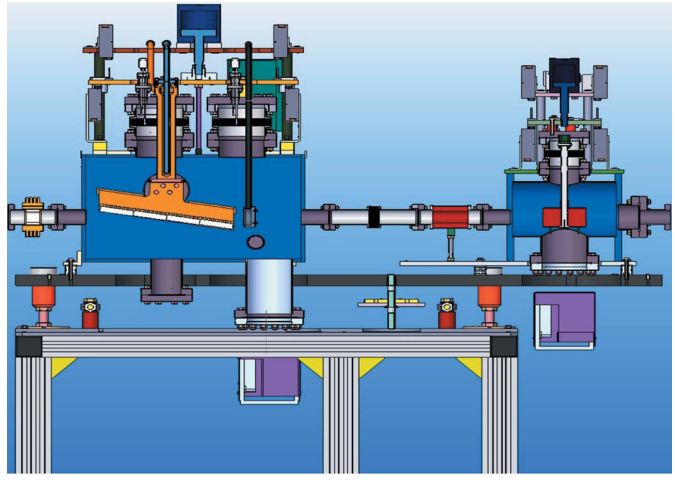

Figure 3
A rendering of the shutter system in the XS3 shaft building and at the end of the XTD9 tunnels. The beam comes from left to right. It hits a boron carbide absorber in grazing-incidence geometry in order to distribute the heat load. Behind the absorber is the burn-through monitor as described in the text. The 8 cm-thick tungsten block in the separate vacuum chamber on the right absorbs the high-energy spontaneous radiation.

X-ray beam in air. The shutters were designed to withstand 300 pulses per pulse train of the unfocussed X-ray beam. As the facility will increases its performance in the future, the number of pulses impinging on a closed shutter will have to be restricted.

3. Vacuum system

The SASE1 beam transport vacuum system encloses the ~1.2 km-long beam path by an ultrahigh vacuum. The entire system is windowless and connects the vacuum of the instruments to the vacuum of the undulator and linear accelerator up to the injector. Fast valves located towards the undulator vacuum and the instruments ensure the integrity of the remaining vacuum system in case of a vacuum breach. In addition to the fast valves, gate valves are used to divide the beam transport system into sections with a maximum of 180 m length. The vacuum system is controlled by a programmable logic controller (PLC) system. Monitoring and changes of parameters can be done via the *Karabo* controls software (Hauf *et al.*, 2019; Heisen *et al.*, 2013). If the vacuum control system detects a pressure above threshold along the vacuum system, the two gate valves before and after the detected area are closed. Because the FEL beam could damage these valves, a signal is sent to the machine protection that stops the beam. For the fast valves, the time to stop the beam is about 30 µs, much faster than the closing time of the valves of 20 ms. For the regular gate valves, the signal is processed in the vacuum PLC leading to a shut-off time with a maximum of 100 ms.

The base pressure in the vacuum system is typically better than 10^{-8} mbar with the threshold set to a maximum of 5×10^{-6} mbar. Special care was taken in selecting materials and cleaning all vacuum components according to the European XFEL vacuum guidelines before the installation (Dommach, 2015). Thirty metres around each mirror, the vacuum sections are specified as particle-free. The assembly in these areas was performed with movable clean tents according to the ISO 6 clean-room standard, locally reaching to ISO 5, and the air quality was monitored with a particle counter during the installation. To avoid particle production during the assembly no silver-coated screws are used, but instead stainless steel screws are used with copper or titanium nuts. Around the mirror chambers, permanent clean-tents are installed that allow faster access to the mirrors.

No bake-out of the system is performed because of the size of the vacuum system and the sensitivity of the mirrors. Venting sections of the vacuum system is carried out by evaporated liquid nitrogen through particle filters. After venting, the recovery time of a vacuum section is typically 24 h.

Copper gaskets are used throughout the beam transport system to ensure the ultrahigh-vacuum standard under radiation environment. Only the gate valves inbetween vacuum sections have Viton seals.

The vacuum system is pumped by ion pumps, located a maximum of 32 m apart in the long vacuum sections with 100 mm-diameter vacuum pipes. For smaller beam-pipe diameters and in the vicinity of beam-intersecting components, a higher density of ion pumps is required to reach the vacuum base pressure. Before and after the sections of the gas-based diagnostics, the differential pumps with turbo pumps and oil-free pre-pumps are used.

4. High-precision mirrors

The offset and distribution mirrors have enhanced requirements concerning slope error and profile error with respect to standard mirrors used at synchrotron radiation sources. At the SASE1 beamline, the beam-transport mirrors are located 250–350 m away from the source, about ten times farther than mirrors at a standard synchrotron radiation facility. With a comparable source size in the undulator, this leads to roughly a ten-time tighter requirement on the slope error. In addition, because of the high degree of coherence of the FEL radiation, all parts of the beam can interfere with each other, leading to a requirement of a maximum height error deviation across the full length of the mirror (Samoylova *et al.*, 2009, 2016; Yashchuk *et al.*, 2015). For the beam-transport mirrors, a slope error of 50 nrad r.m.s. and a profile error of 2 nm peak-to-valley were specified (Sinn *et al.*, 2011). At the same time, mirror lengths of about 1 m are required to transport at least 4σ of the beam for all energies. This combination of requirements posed a new challenge to mirror manufacturers, which was only overcome in 2016, when the first of such mirrors was delivered to European XFEL. Preserving the profile error specifications for the mirror mounted to its holder and performing metrology on this level of accuracy brings additional challenges. Fig. 4 shows a mirror profile measured with a 30 cm-diameter Fizeau interferometer at the metrology laboratory of the European XFEL (Vannoni *et al.*, 2016*a*,*b*). The measurements were performed in normal incidence, which required seven sub-aperture measurements stitched together. The measurement in Fig. 4 shows a peak-to-valley of 5 nm, which is larger than the peak-to-valley value of 2 nm measured by the vendor for this mirror. We attribute this difference to residual stress coming from the mirror mount and to the limitations of our metrology.

Before installation, a map of the entire optical area of each mirror was measured. In this way, changes to the mirror profile or its surface caused by interaction with the beam could be investigated later. At the end of 2017, the M2 mirror had to be exchanged because of a failure of the bending mechanism. No damage or alterations of this mirror could be observed after about six months of operation although with limited beam power.

All mirrors of the SASE1 beam transport were coated with a 60 nm-thick layer of boron carbide to ensure maximum reflectivity and the highest durability against beam damage. The thickness variation achieved was below 1 nm peak-to-valley for boron carbide films along the entire mirror length (Störmer *et al.*, 2016, 2018). Metrology measurements before and after the coating demonstrated no negative effect of the coating on the mirror shape.

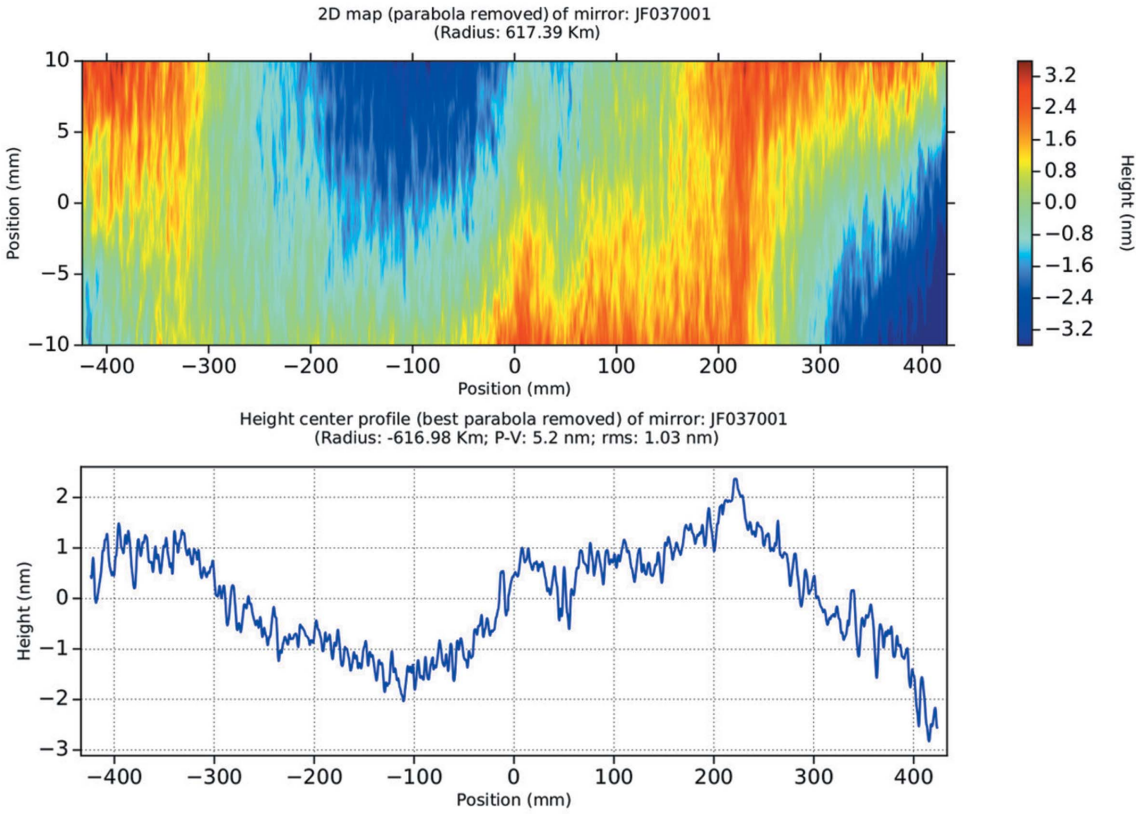

Figure 4
The results of a measurement of the SASE1 M1 mirror with a Fizeau interferometer. The top panel shows a 2D map of the entire polished area, the lower panel shows the height profile on the centre line.

5. Beam-profile measurements

The beam quality at the end of the SASE1 beamline was investigated by beam-profile measurements for individual X-ray pulses and averaging over many pulses (Music, 2018). The top panel of Fig. 5 shows the beam in front of the SPB shutter averaged over 541 FEL pulses with M1 and M2 in the beam. The vertical structures visible in the beam profile come from the combined figure errors of M1 and M2 and are consistent with the metrology data obtained from the mounted substrates. The absence of circular structures proves that there are no dust particles of large enough size to distort the beam on the mirror surfaces. After inserting the collimating CRLs (Fig. 5, middle panel), the beam profile shrinks in the vertical and horizontal directions. The absence of horizontal stripes or additional vertical stripes demonstrates that the CRLs do not add an additional phase error in this configuration. In the bottom panel of Fig. 5, the CRLs are removed; instead, the M2 is tuned from the flat position to optimum focusing on the imager. The full width half-maximum of the obtained profile is about 330 µm in the horizontal direction.

The analysis of pulse-to-pulse variation of the beam position in the top panel of Fig. 5 revealed a fluctuation of about 1.5 mm in horizontal and vertical directions, which corresponds to pointing fluctuations on the scale of microradians. Note that the accelerator was running in single-pulse mode without intra-bunch feedback, which was added only later to the standard operation mode.

6. Conclusion and outlook

The early experience with the beam and during the user period demonstrated that the reliability of the overall system is extremely high and only a few unplanned tunnel accesses were required during the first 18 months of commissioning and operation. The optical quality of the mirrors and the CRLs is on a very high level and fulfils the tight specifications imposed by the coherence of the beam and the very long beam paths. The cleanliness of the vacuum system seems to be sufficient because neither blacking of the mirrors during the first months of operation nor dust particles distorting the beam profiles were observed. An improvement of the beam-profile quality can be achieved by further optimization of mirror-polishing methods and reduction of distortions by the holder.

One aspect that clearly needs to be improved is the beam-position stability at the experiments on different time scales. Stabilizing the FEL beam by additional feedbacks to the electron beam in the undulator section and improving the mirror chamber stability can potentially minimize fluctuations and drifts. One challenge is to extract reliable photon-beam-position signals on the relevant time scales compatible with full train operation and not limiting the beam quality. Fluctuations on the time scale of seconds could then be fed to the electron orbit, while the piezo actuators of the mirrors M2 and M3 could correct slower drifts.

A major goal of the further development of the SASE1 beam transport is to increase the number of pulses per train.

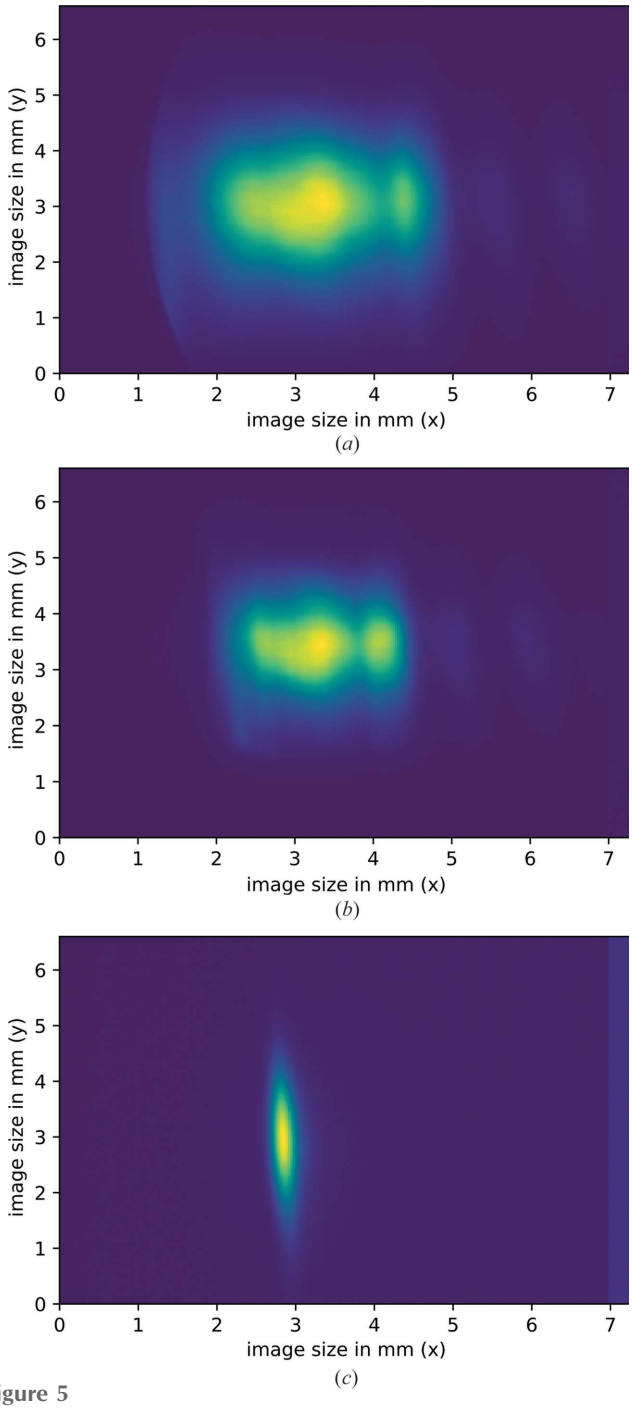

Figure 5
Images of the beam at the end of the SPB beamline at 9.3 keV. (Top) The M2 bender is flat with no CRL in the beam. The measured beam size is 2.4 mm × 2.0 mm. (Middle) A collimating CRL was inserted resulting in a 22% reduced beam size of 1.8 mm × 1.6 mm. (Bottom) No CRLs are in the beam, but the M2 bender is focusing on the imager. The beam size is now 0.33 mm × 1.52 mm.

The user operation started in 2017 with 30 pulses per train, which was increased by the end of 2018 in several steps to 300 pulses per train. For each increase of allowed power level, safety tests are required that can prove that the concepts of beam stopping and radiation shielding are still valid. Furthermore, the available photon energy range at SASE1 will be expanded towards the 20 keV range.

Acknowledgements

We would like to thank the European XFEL groups – Advance Electronics (AE), Control and Analysis Software (CAS), and X-Ray Photon Diagnostics (XPD) – as well as the DESY groups – MKK, MEA, MPS and D3 – for their contributions during the construction phase of the beamline; the members of the photon commissioning team; Frank Siewert for frequent discussions on metrology data; Tino Noll for discussions on the development of the mirror chamber design; and Mikhail Yurkov and Evgueni Schneidmiller for discussions on SASE beam properties. Furthermore, we thank Klaus Giewekemeyer and Peter Zalden for their support in measuring the beam images in Fig. 5.

References

Abeghyan, S., Bagha-Shanjani, M., Chen, G., Englisch, U., Karabekyan, S., Li, Y., Preisskorn, F., Wolff-Fabris, F., Wuenschel, M., Yakopov, M. & Pflueger, J. (2019). *J. Synchrotron Rad.* **26**, 302–310.

Altarelli, M., Brinkmann, R., Chergui, M., Decking, W., Dobson, B., Düsterer, S., Grübel, G., Graeff, W., Graafsma, H., Janos Hajdu, Jonathan Marangos, J. P., Redlin, H., Riley, D., Robinson, I., Rossbach, J., Schwarz, A., Tiedtke, K., Tschentscher, T., Vartaniants, I., Wabnitz, H., Weise, H., Wichmann, R., Karl Witte, A. W., Wulff, M. & Yurkov, M. (2006). *The European X-ray Free-Electron Laser.* Technical Design Report, DESY 2006-097. DESY, Hamburg, Germany.

Aquila, A., Sobierajski, R., Ozkan, C., Hájková, V., Burian, T., Chalupský, J., Juha, L., Störmer, M., Bajt, S., Klepka, M. T., Dłużewski, P., Morawiec, K., Ohashi, H., Koyama, T., Tono, K., Inubushi, Y., Yabashi, M., Sinn, H., Tschentscher, T., Mancuso, A. P. & Gaudin, J. (2015). *Appl. Phys. Lett.* **106**, 241905.

Bressler, C. (2011). European XFEL Technical Report, XFEL.EU TR-2011-005. European XFEL Facility, Hamburg, Germany.

Decking, W. *et al.* (2019). Submitted.

Dommach, M. (2015). European XFEL Technical Note, XFEL.EU TN-2011-001-05. European XFEL Facility, Hamburg, Germany

Dong, X., Shu, D. & Sinn, H. (2016). *AIP Conf. Proc.* **1741**, 040027.

Freijo Martín, I., Vannoni, M., Music, V., Sinn, H. (2016). *Proc. SPIE*, **9965**, 996504.

Galler, A., Gawelda, W., Biednov, M., Bömer, C., Britz, A., Brockhauser, S., Choi, T.-K., Diez, M., Frankenberger, P., French, M., Göries, D., Hart, M., Hauf, S., Khakhulin, D., Knoll, M., Korsch, T., Kubicek, K., Kuster, M., Lang, P., Lima, F. A., Ott, F., Schulz, S., Zalden, P. & Bressler, C. (2019). *J. Synchrotron Rad.* **26**. To be published.

Gerasimova, N., Sinn, H., Dziarzhytski, S. & Treusch, R. (2014). *Proceedings of the 36th International Free-Electron Laser Conference (FEL 2014)*, 25–29 August 2014, Basel, Switzerland.

Grünert, J., Carbonell, M. P., Dietrich, F., Falk, T., Freund, W., Koch, A., Kujala, N., Laksman, J., Laksman, J., Tiedtke, K., Jastrow, U. F., Sorokin, A., Syresin, E., Grebentsov, A. & Brovko, O. (2019). *J. Synchrotron Rad.* **26**. To be published.

Hauf, S., Heisen, B., Aplin, S., Beg, M., Bergemann, M., Bondar, V., Boukhelef, D., Danilevsky, C., Ehsan, W., Essenov, S., Fabbri, R., Flucke, G., Marsa, D. F., Göries, D., Giovanetti, G., Hickin, D., Jarosiewicz, T., Kamil, E., Khakhulin, D., Klimovskaia, A., Kluyver, T., Kirienko, Y., Kuhn, M., Maia, L., Mamchyk, D., Mariani, V., Mekinda, L., Michelat, T., Münnich, A., Padee, A., Parenti, A., Santos, H., Silenzi, A., Teichmann, M., Weger, K., Wiggins, J., Wrona, K., Xu, C., Youngman, C., Zhu, J., Fangohr, H. & Brockhauser, S. (2019). *J. Synchrotron Rad.* **26**. To be published.

Heisen, B. C., Boukhelef, D., Esenov, S., Hauf, S., Kozlova, I., Maia, L., Parenti, A., Szuba, J., Weger, K., Wrona, K. & Youngman, C. (2013). *Proceedings of the 14th International Conference on*

Accelerator and Large Experimental Physics Control Systems (ICALEPCS 2013), San Francisco, California, USA.
Mancuso, A. P., Aquila, A., Batchelor, L., Bean, R. J., Bielecki, J., Borchers, G., Doerner, K., Giewekemeyer, K., Graceffa, R., Kelsey, O. D., Kim, Y., Kirkwood, H. J., Legrand, A., Letrun, R., Manning, B., Lopez Morillo, L., Messerschmidt, M., Mills, G., Raabe, S., Reimers, N., Round, A., Sato, T., Schulz, J., Signe Takem, C., Sikorski, M., Stern, S., Thute, P., Vagovič, P., Weinhausen, B. & Tschentscher, T. (2019). *J. Synchrotron Rad.* **26**, 660–676.
Manetti, M., Buzmakov, A., Samoylova, L., Schneidmiller, E., Sinn, H., Szuba, J., Wrona, K. & Yurkov, M. (2019). *AIP Conf. Proc.* **2054**, 030019. (See also web application available here: https://in.xfel.eu/fastxpd.)
Music, V. (2015). Bachelor's Thesis, University of Hamburg, Germany.
Music, V. (2018). Master's Thesis, University of Hamburg, Germany.
Noll, T., Holldack, K., Reichardt, G., Schwarzkopf, O. & Zeschke, T. (2009). *Prec. Eng.* **33**, 291–304.
Noll, T., Sinn, H. & Trapp, A. (2016). *Proceedings of the 9th Mechanical Engineering Design of Synchrotron Radiation Equipment and Instrumentation (MEDSI 2016)*, 11–16 September 2016, Barcelona, Spain, pp. 121–123.
Samoylova, L., Buzmakov, A., Chubar, O. & Sinn, H. (2016). *J. Appl. Cryst.* **49**, 1347–1355.
Samoylova, L. & Sinn, H. (2014). *Proc. SPIE*, **9209**, 920904.
Samoylova, L., Sinn, H., Siewert, F., Mimura, H., Yamauchi, K. & Tschentscher, T. (2009). *Proc. SPIE*, **7360**, 73600E.
Sinn, H., Dommach, M., Dong, X., La Civita, D., Samoylova, L., Villanueva, R. & Yang, F. (2012). European XFEL Technical Design Report, XFEL.EU TR-2012-006. European XFEL Facility, Hamburg, Germany
Sinn, H., Gaudin, J., Samoylova, L., Trapp, A. & Galasso, G. (2011). Conceptual Design Report, XFEL.EU TR-2011-002. European XFEL Facility, Hamburg, Germany
Snigirev, A., Kohn, V., Snigireva, I. & Lengeler, B. (1996). *Nature*, **384**, 49–51.
Störmer, M., Siewert, F., Horstmann, C., Buchheim, J. & Gwalt, G. (2018). *J. Synchrotron Rad.* **25**, 116–122.
Störmer, M., Siewert, F. & Sinn, H. (2016). *J. Synchrotron Rad.* **23**, 50–58.
Tiedtke, K., Azima, A., von Bargen, N., Bittner, L., Bonfigt, S., Düsterer, S., Faatz, B., Frühling, U., Gensch, M., Gerth, C., Guerassimova, N., Hahn, U., Hans, T., Hesse, M., Honkavaar, K., Jastrow, U., Juranic, P., Kapitzki, S., Keitel, B., Kracht, T., Kuhlmann, M., Li, W. B., Martins, M., Núñez, T., Plönjes, E., Redlin, H., Saldin, E. L., Schneidmiller, E. A., Schneider, J. R., Schreiber, S., Stojanovic, N., Tavella, F., Toleikis, S., Treusch, R., Weigelt, H., Wellhöfer, M., Wabnitz, H., Yurkov, M. V. & Feldhaus, J. (2009). *New J. Phys.* **11**, 023029.
Tschentscher, T., Bressler, C., Grünert, J., Madsen, A., Mancuso, A. P., Meyer, M., Scherz, A., Sinn, H. & Zastrau, U. (2017). *Appl. Sci.* **7**, 592.
Vannoni, M. & Freijo Martin, I. (2016*a*). *Metrologia*, **53**(1), 1–6.
Vannoni, M. & Freijo Martín, I. (2016*b*). *Rev. Sci. Instrum.* **87**, 051901.
Vannoni, M., Freijo Martín, I. & Sinn, H. (2016). *J. Synchrotron Rad.* **23**, 855–860.
Vannoni, M., Freijo Martín, I., Music, V. & Sinn, H. (2016). *Opt. Express*, **24**, 17292–17302.
Yashchuk, V., Samoylova, L. & Kozhevnikov, I. (2015). *Opt. Eng.* **54**, 025108.